

# Kinematic Source Parameters for the 1989 Loma Prieta Earthquake from the Nonlinear Inversion of Accelerograms

by Antonio Emolo and Aldo Zollo

**Abstract** We describe a technique to infer the kinematic parameters of the earthquake rupture process by the nonlinear inversion of near-source high-frequency seismic records. The model assumes that each point on the fault plane slips, when the rupture front passes, with a variable slip amplitude. For a given rupture model synthetic seismograms are computed by using the ray theory and a plane-layered velocity structure. The rupture velocity and the final slip are specified at a set of control points on the fault plane and the values at any point on the fault are then obtained by a bicubic interpolation. The final slip and rupture velocity at the fault-grid nodes are determined by searching for the minimum of a misfit function by using the Genetic Algorithm. The number of control points is progressively increased to move from a high- to low-wavelength description of final slip and rupture velocity on the fault plane. The optimal model parameter set is chosen according to the minimum of the corrected Akaike Information Criterion parameter. The uncertainty on the source parameters has been estimated through the analysis of cross-correlation of the misfit function in the neighborhood of the final, best-fit, rupture model. The method is applied to near-source, strong motion records of the 1989 Loma Prieta earthquake. We find that the most earthquake slip occurred in two regions located northwest and southeast of the hypocenter, consistent with previous models obtained using other data and techniques. Moreover, we find that the rupture propagated faster toward the southeast than in the northwest direction. The total duration of the rupture is found to be approximately 9 sec.

## Introduction

One main target of observational seismology is to estimate the earthquake source characteristics from the recorded ground motion. Near-source seismological observations (distances comparable with the fault length) of moderate to large earthquakes (magnitude greater than 6) indicate that the fracture-process heterogeneity (nucleation, propagation, and arrest of a rupture on the fault surface) strongly affects the seismic radiation at frequencies higher than 1 Hz (Heaton, 1990; Anderson, 1991; Koyama, 1997; Bouchon *et al.*, 2002).

Several theoretical and observational studies have been performed to investigate the propagation of short-period waves in a realistic, heterogeneous earth structure. The results of these studies show that high-frequency waves excited by a heterogeneous source process can be contaminated by the scattering and attenuation effects along the propagation path (Koyama, 1997). The *a priori* knowledge of the elastic/anelastic properties of the propagation medium is therefore an essential condition for a high-resolution source modeling.

The study of the rupture process through the modeling

of the observed seismic radiation, in general, is done by adopting a kinematic approach to describe the seismic source (Beroza and Spudich, 1988; Zhang *et al.*, 2003). The kinematic description of the earthquake source has the advantage of using a limited number of parameters to characterize the source, such as fault size, the final slip distribution on the fault, the rupture velocity, and the slip duration (rise time). Nevertheless, even using a simplified kinematic description of the rupture process, the problem of inverting short-period records is strongly nonlinear when considering variable rupture velocity and/or rise time on the fault. The insufficient data coverage of the source can be the cause for nonuniqueness of solution. The most pathological effect is the trade-off between the slip rate and rupture-velocity distribution on the fault, which leads to similar perturbations on the seismic waveforms.

This article addresses the problem of retrieving the space-time slip function from the inversion of short-period earthquake records and of quantitatively assessing the uncertainty and resolution on the estimated rupture model parameters. We consider an approach based on a kinematic

description of the rupture process that uses a nonlinear optimization technique, the Genetic Algorithm, to explore the space of the kinematic model parameters, that is, final slip and rupture velocity (we consider the rise-time constant on the fault) at control points of an interpolation function on the rupture plane.

### The Forward Problem and Model Parameterization

The far-field approximation of the representation integral is used to compute synthetic seismograms for an extended earthquake rupture. The high-frequency approximation of the wave field allows us to compute in a fast and accurate way the Green's functions of body waves propagating in 1D and 3D media (Farra *et al.*, 1986; Farra and Madariaga, 1987). Other numerical methods for computing the Green's functions are proposed and applied in the literature, for example, the discrete wave-number method of Bouchon (1979, 2003), the Empirical Green Function method of Hartzell (1978), Irikura (1986), and Hutchings (1994). Nevertheless, these methods can be very time consuming when implemented in a nonlinear waveform inversion code.

The ray theory synthetics can be considered a good representation of the seismic wave field at near-source distances if the dominant signal wavelengths are smaller than receiver distances from the source (Bernard and Madariaga, 1984; Farra *et al.*, 1986). In our case, this approximation is valid at distances less than a few source depths so that the surface waves are not important. In these cases the direct  $S$  waves emitted by the seismic rupture become dominant in amplitude on seismograms relative to near-field terms and secondary arrivals (Farra *et al.*, 1986; Beroza and Spudich, 1988; for the Loma Prieta earthquake case study, Zeng *et al.*, 1993; Beroza, 1996).

At high frequencies, the ground displacement associated with the wave type  $c$  ( $P$  or  $S$ ) at a given receiver located at  $\mathbf{x}$  can be obtained as the summation of signals emitted by elementary sources (subfaults) densely distributed on the rupturing surface:

$$\mathbf{u}^c(\mathbf{x}, t) = \sum_{m,n} \mathbf{u}_{m,n}^c(\mathbf{x}, t), \quad (1)$$

where the ground displacement produced by the subfault  $(m, n)$ ,  $\mathbf{u}_{m,n}^c$ , is given by the representation integral (Aki and Richards, 1980):

$$\mathbf{u}_{m,n}^c(\mathbf{x}; t) = \int \int_{\text{subfault}} \mathbf{G}_{m,n}^{\text{FF}}(\mathbf{x}, \xi; t, 0) * \Delta \dot{u}_{m,n}(\xi; t - T_{m,n}^c) d\Sigma. \quad (2)$$

In (2),  $\mathbf{G}_{m,n}^{\text{FF}}$  is the Green's function in the far-field approximation,  $\Delta \dot{u}_{m,n}$  is the slip rate,  $T_{m,n}^c$  represents the travel time for the wave  $c$  from the elementary source located in  $\xi_{m,n}$  to

the receiver, and the symbol  $*$  indicates the convolution operation.

The asymptotic Green's functions for direct body waves in a flat-layered propagation medium are computed with the numerical kernel developed by V. Farra and based on the original formulation by Farra *et al.* (1986). In this approach the focal mechanism is *a priori* fixed but the radiation pattern coefficient (which is included in function  $\mathbf{G}$ ) is variable on the fault, depending on the relative position of the radiating subfault and receiver.

To account for the Earth anelasticity, the Green's function is convolved with the Azimi's attenuation function (Azimi *et al.*, 1968) parameterized by a constant quality factor  $Q_c$ . The slip-velocity function in equation (2) is approximated by a boxcar function:

$$\Delta \dot{u}(\xi; t) = \begin{cases} \frac{D(\xi)}{\tau(\xi)} & \text{for } T_R(\xi) < t < T_R(\xi) + \tau(\xi) \\ 0 & \text{elsewhere} \end{cases} \quad (3)$$

where  $T_R(\xi)$ ,  $\tau(\xi)$ , and  $D(\xi)$  are, respectively, the rupture time, the rise time, and the final slip associated with the fault element whose position is  $\xi$ .

According to equations (1), (2), and (3), the displacement recorded at  $\mathbf{x}$  is linearly related to the slip intensity  $D$ , once the rupture-time distribution is assigned. However, the rupture time  $T_R$  implicitly appears in the slip-rate definition, which makes the dependence of observed displacement on the rupture-velocity parameter strongly nonlinear. In this study we adopted a truly nonlinear approach for estimating the source parameters from seismic waveform data by the whole exploration of the model parameter space with a nonlinear optimization technique. This approach is rather different from the ones used by previous authors who solved the inverse problem through a trial-and-error forward modeling (Archuleta, 1984) or by a linearized iterative approach (Beroza and Spudich, 1988).

The model parameters are the values of the final slip and rupture velocity at a set of control points of a bicubic interpolating function, regularly distributed on the fault surface. The interpolation allows us to determine the final slip- and rupture-velocity distributions on the whole fault at the fine grid spacing required to avoid undesired spatial aliasing effects.

The computation of synthetic seismograms by equation (1) requires the estimation of rupture times on the fault. For a heterogeneous rupture-velocity distribution and a given nucleation point, the rupture front propagates having an irregular shape. In this case, the problem of computing rupture times can be solved by tracing the rupture propagation fronts along the fault and searching for the first arrival at each point of the rupturing surface. We used the 2D finite-difference code of Podvin and Lecomte (1991) for computing the rupture times, assuming that the eikonal equation can describe the rupture front evolution on the fault.

### The Inverse Problem and Inversion Strategy

The inverse problem is solved by searching the maximum of a fitness function by a wide exploration of the model parameter space. The search is performed by the Genetic Algorithm (GA) (Goldberg, 1989; Charbonneau, 1995). Among the different nonlinear optimization techniques (e.g., simulated annealing, Monte Carlo search), GA is revealed to be very efficient and fast for a wide exploration search in a multidimension model space and for bracketing the region containing the absolute maximum (Sambridge and Drijkoningen, 1992; Boschetti *et al.*, 1996; Zollo *et al.*, 2002). A complete description of GA (Pikaia routine) and its parameters can be found in Charbonneau (1995).

Let us now consider a set of  $N_S$  seismic stations that have recorded an earthquake and let us indicate with  $S^{\text{obs}}$  the corresponding seismic records. Each record will consist of  $N_C$  components (with  $1 \leq N_C \leq 3$ ) and  $N_T$  time samples. Let us indicate with  $S^{\text{theo}}$  the synthetic seismograms evaluated for a given model parameters set. The fitness function to be maximized by using the GA is defined as

$$F = \frac{E_{\text{MAX}} - E}{E_{\text{MAX}}}, \quad (4)$$

where

$$E = \frac{\sum_{i=1}^{N_S} \sum_{j=1}^{N_C} \sum_{k=1}^{N_T} (S_{ijk}^{\text{obs}} - S_{ijk}^{\text{theo}})^2 \left| S_{ijk}^{\text{theo}} \right|}{\sum_{i=1}^{N_S} \sum_{j=1}^{N_C} \sum_{k=1}^{N_T} \left| S_{ijk}^{\text{theo}} \right|} \quad (5)$$

and  $E_{\text{MAX}}$  represents the maximum allowed value for the cost function (5). In other words, the individuals of the initial population on which the GA acts all have a cost  $E \leq E_{\text{MAX}}$ . The parameter  $E_{\text{MAX}}$  can be chosen arbitrarily. In our application, after performing several preliminary tests, we chose for  $E_{\text{MAX}}$  a value of  $0.05 \text{ m}^2 \text{ sec}^{-2}$ , which corresponds to the cost associated with a homogeneous rupture model (i.e., a model characterized by homogeneous final slip- and rupture-velocity distributions). On the basis of equation (4), we explicitly note that the function  $F$  assumes a value equal to zero if  $E = E_{\text{MAX}}$ , whereas it reaches a maximum value equal to 1 if  $E = 0$  (i.e., if the synthetic seismograms exactly match the real seismograms).

For computing the misfit function (equation 5), synthetic and observed seismograms are lined up after cross-correlating the two records and relatively shifting the traces by the time-lag corresponding to the maximum of the cross-correlation function. Several optimization runs are performed by progressively increasing the density of grid points in which the slip and rupture velocity are evaluated through the data inversion and which coincide with the control points of the bicubic interpolating function. At very early stages in which the number of control points on the fault is small, the

optimization is performed over a wide range of allowed final slip- and rupture-velocity values. In the subsequent runs, when the number of control points is progressively increased, the search is performed with smaller and smaller allowed variations for final slip and rupture velocity around the model estimated in the previous run. This strategy for model space reconstruction is, in principle, equivalent to moving from a high- to low-wavelength description of the slip- and rupture-velocity distributions on the fault plane. This approach has been widely used in seismic tomography (Lutter *et al.*, 1990) and in migration techniques where it is known as the multiscale approach (Bunks *et al.*, 1995; Jin and Beydoun, 2000). The optimization procedure has been validated by synthetic tests assuming both heterogeneous and homogeneous final slip- and rupture-velocity distributions on the fault plane and both regular and sparse receiver around the source (Emolo, 2001). In particular, the choice of progressively increasing the number of control points makes the estimation of model parameters robust and efficient by reducing the computational costs.

A point that needs to be considered concerns the evaluation of the statistical significance of models described by a different number of parameters. An objective criterion must be defined according to which one can decide whether stopping or continuing the optimization process by increasing the control points density. This point is addressed by the corrected Akaike Information Criterion (AICc) that was first introduced by Akaike (1974) for model selection and recently modified from its original formulation by Cavanaugh (1997). The criterion states that, among the best-fit models described by a different number of parameters, the one that minimizes the function has to be selected:

$$\text{AICc} = N \ln(2\pi E) + \frac{N(N + P)}{N - P - 2}. \quad (6)$$

In equation (6),  $E$  represents the misfit value,  $N$  is the number of data, and  $P$  is the number of parameters. The search for a minimum AICc corresponds to finding the best compromise between fit quality and simplicity of the model (small number of parameters). By introducing this criterion the problem of selecting the optimal model parameterization is formulated without the need for the subjective decision required in the classical approaches based on the “test of hypothesis” or a variance comparison. When two models described by a different number of parameters provide the same misfit value, the one defined by the smaller number of parameters is chosen. In other words, the search for the minimum of the AICc parameter provides a mathematical formulation of the Occam’s razor principle, also known as the principle of parsimony in model building.

### The Loma Prieta Earthquake

The Loma Prieta earthquake ( $M_L$  6.7,  $M_S$  7.1) occurred at 00:04:15.2 UTC on 18 October 1989, at latitude

37.036° N, longitude 121.883° W, and at 17 km depth (Dietz and Ellsworth, 1990) southwest of the southern Santa Cruz Mountains section of the San Andreas fault. The scalar seismic moment estimates range between  $1.7 \times 10^{19}$  N m and  $3.4 \times 10^{19}$  N m (Kanamori and Satake, 1990). Aftershocks occurred on both sides of the fault relative to the hypocenter for a distance of approximately 50 km, filling a seismic gap (U.S. Geological Survey, 1990). The locations of aftershocks with respect to the hypocenter suggest that the rupture propagated bilaterally along the strike and unilaterally up-dip (Beroza, 1996).

The 1989 Loma Prieta earthquake has been the object of numerous studies that used teleseismic records to determine the source characteristics (Barker and Salzberg, 1990; Choy and Boatwright, 1990; Kanamori and Satake, 1990; Langston *et al.*, 1990; Romanowicz and Lyon-Caen, 1990; Ruff and Tichelaar, 1990; Zhang and Lay, 1990). All these studies indicate that slip occurred on a fault dipping approximately 70° and striking approximately 130°. The rake, determined from teleseismic data analysis, is approximately 140° (Zhang and Lay, 1990).

According to Beroza (1996), the fault plane used in our study extends from 15 km northwest to 20 km southeast of the hypocenter. The dipping fault plane intersects the hypocenter at a depth of 18 km, with a strike of 130° and a dip of 70° southwest. The modeled extent of the rupture zone in the up-dip direction from the hypocenter is 14 km, corresponding to depths from 18 km to slightly less than 5 km.

The velocity model used to compute the Green's functions is reported in Table 1. This model, given by Beroza (1996), was determined by Dietz and Ellsworth (1990) analyzing the Loma Prieta aftershocks. Because they found a difference in the velocity in the uppermost layer across the San Andreas fault, Beroza (1996) suggested using a slightly different model in the northeast and southwest sides of the fault. The velocity model used in our inversion analysis does not account for specific site effects that could affect the amplitude of signals in the frequency range selected for our study (0.5–5 Hz).

A constant quality factor  $Q_S = 300$  (Boatwright *et al.*, 1991; Chin and Aki, 1991) was used to parameterize the Azimi's attenuation function.

### Strong Motion Data and Data Analysis

The Loma Prieta earthquake occurred in a region densely instrumented with strong motion accelerographs. The locations of stations used in our study are shown in Figure 1 and listed in Table 2. The peak ground accelerations (PGAs) recorded by each instrument are also reported in Table 2. The instrument-corrected acceleration data were integrated to get the ground velocity and bandpass filtered with a four-pole zero-phase Butterworth filter with corner frequencies at 0.5 and 5.0 Hz. The low-frequency limit was constrained by the requirement that the receivers have to be a few wavelengths away from the nearest segment of the

**Table 1**  
Characteristics of the Propagation Medium Used in this Study (after Beroza, 1996)

Depth (m)	P-wave Velocity (m/sec)	S-wave Velocity (m/sec)	Density (kg/m <sup>3</sup> )
Northeast of Fault			
0.0	3340	1930	2.5
1,100	5010	2890	2.7
9,100	6260	3610	2.7
24,500	6950	4010	2.8
Southeast of Fault			
0.0	3420	1970	2.5
1,100	4580	2640	2.7
9,100	6260	3610	2.7
24,500	6950	4010	2.8

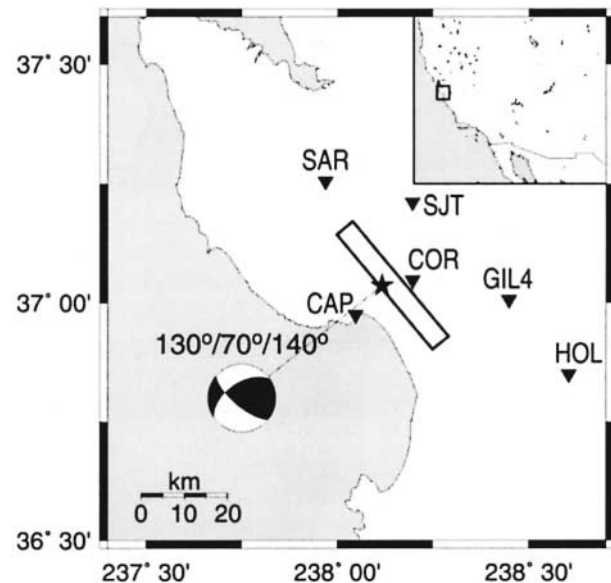


**Figure 1.** Locations of the strong motion stations used in this study. The rectangle represents the surface-fault projection, and the star is the Loma Prieta earthquake epicenter. The fault-plane solution according to Zhang and Lay (1990) is also shown.

**Table 2**  
Strong Motion Stations Used in Our Analysis

Code	Organization	Location	PGA (ms <sup>-2</sup> )
CAP	CDMG	Capitola Fire Station	5.00
COR	CDMG	Corralitos	6.18
GIL4	CDMG	Gilroy array, station 4	4.08
HOL	USGS	Hollister City Hall	3.62
SAR	CDMG	Aloha Avenue, Saratoga	4.15
SJT	CDMG	Santa Theresa Hills, San Jose	2.69

Organizations: CDMG, California Division of Mines and Geology; USGS, U.S. Geological Survey.

fault (Spudich and Frazer, 1984; Farra *et al.*, 1986). The high-frequency corner is arbitrarily chosen and represents a tentative high-frequency limit of our deterministic modeling.

Receivers located within about 40-km epicentral distance have been considered because our modeling is limited to the direct *S* waves. Somerville and Yoshimura (1990), Chin and Aki (1991), and, in particular for the Loma Prieta case, Zeng *et al.* (1993) demonstrated that complex propagation effects (dominant secondary arrivals, multipathing) are minimized in this distance range. A window delimiting the direct *S* arrival has been selected from the horizontal components of the ground velocity and used for the inversion analysis. To avoid inaccuracies on travel-time evaluation and hypocentral location due to the use of a 1D velocity model, we decided to perform the waveform modeling in the time window

$$[T_{S,i}, T_{S,i} + \Delta T_i],$$

where *i* is the station index,  $T_{S,i}$  is the first *S*-arrival time measured from the record origin time, and  $\Delta T_i$  is the estimated duration of the direct *S* wave field radiated by the Loma Prieta earthquake fault. The first *S* arrival and the direct *S*-wave window have been identified on each record through a visual inspection and *S*-wave polarization analysis on filtered velocity and displacement records (Fig. 2).

### Results of the Inversion

The parameterization of the rupture process allows each subfault on the fault to slip once when the rupture front passes, with a spatially variable slip amplitude. The rise time in equation (3) is assumed to be smaller than the low-pass frequency of our modeling and it is not determined by the data inversion.

The representation integral (equation 1) was solved numerically by discretizing the fault plane in  $50 \times 50$  m<sup>2</sup> subfaults to avoid undesired spatial aliasing effects (Zollo *et al.*, 1997). The rupture velocity and the final slip distributions on the fault were determined at this fine grid by bicubic spline interpolation of the values obtained by the data inversion at the control points. The initial run of the inversion procedure was performed starting from homogeneous models both for rupture velocity ( $v_R = 2700$  m/sec, mean value after Beroza, 1996) and for final slip (at 1.70 m, according to an average estimate of the scalar seismic moment) with five control points in the strike direction and three control points in the dip direction. Let us explicitly note that two model parameters are associated to each control point: one for the final slip value and one for the rupture velocity. As a consequence, with  $5 \times 3$  control points we have 30 parameters to be determined through the data inversion. In this first run the slip was allowed to vary between 0 and 10 m, whereas the rupture velocity was allowed to vary between 2300 and 3300 m/sec. Individuals in the initial model population were selected randomly around the uniform starting

models (but allowing quite wide variations) with a maximum misfit value equal to  $0.05 \text{ m}^2 \text{ sec}^{-2}$  (parameter  $E_{MAX}$  in equation 5). The population was composed of 400 elements and the GA made it evolve for 110 generations when the fitness value reached a stable value.

In the following runs, the starting models were chosen around the model obtained in the previous search stage and the inversion was performed allowing smaller and smaller variations around them as the number of control points increased.

Table 3 summarizes the results obtained at the end of each inversion run, and Figure 3 shows the evolution for the final slip distribution over the fault during the multiscale search. The whole optimization process has evolved on 1015 generations and the total number of tested models is greater than  $10^6$ .

The maximum number of control points on the fault used to invert strong motion data was  $17 \times 8$  but the preferred model parameterization, according to the AICc criterion, corresponds to the grid with  $15 \times 8$  control points (Table 3). This grid corresponds to a spatial sampling of the fault of 2500 m in the strike direction and 2000 m in the dip direction. Figure 4A and B show, respectively, the final slip and rupture-time distributions on the fault plane for this model. The mean value of the final slip on the fault for this grid is equal to 1.44 m, which corresponds to a scalar seismic moment of  $2.1 \times 10^{19}$  N m that is compatible with the values range indicated by Kanamori and Satake (1990).

The distribution of the final slip on the fault (Fig. 4A) is characterized by two main asperities located southeast and northwest of the hypocenter. Their locations, extensions and maximum amplitudes (about 4 m for the southeastern one and more than 3 m for the northwestern one) are in good agreement with the results of Beroza (1996) and Wald *et al.* (1996). We notice that the high-slip region located northwest of the hypocenter, differently from other studies, seems not to be so focused. This result could be the effect of both data distribution around the fault and/or of the adopted inversion technique. Moreover, we found another high-slip region near the top middle-western edge of the fault which is probably related to the high amplitude associated with the west-east component of the seismogram recorded at the COR receiver.

The mean rupture velocity value for the best-fit model is 2800 m/sec, which is slightly higher than the mean value obtained by Beroza (1996). From the distribution of the rupture times on the fault (Fig. 4B) it is evident that the rupture advanced faster toward the southeast than in the opposite direction, as retrieved by Horton *et al.* (1996). Finally, the total duration of the rupture is about 9 sec, which is compatible with the value estimated by Beroza (1996).

In Figures 5 and 6 the ground-velocity records in the 0.5- to 5-Hz frequency band are compared with the synthetics computed for the best-fit rupture model at all the considered stations. The fit between synthetic and real seismograms is, in general, quite satisfactory although some discrepancies are found in the peak amplitude values. How-

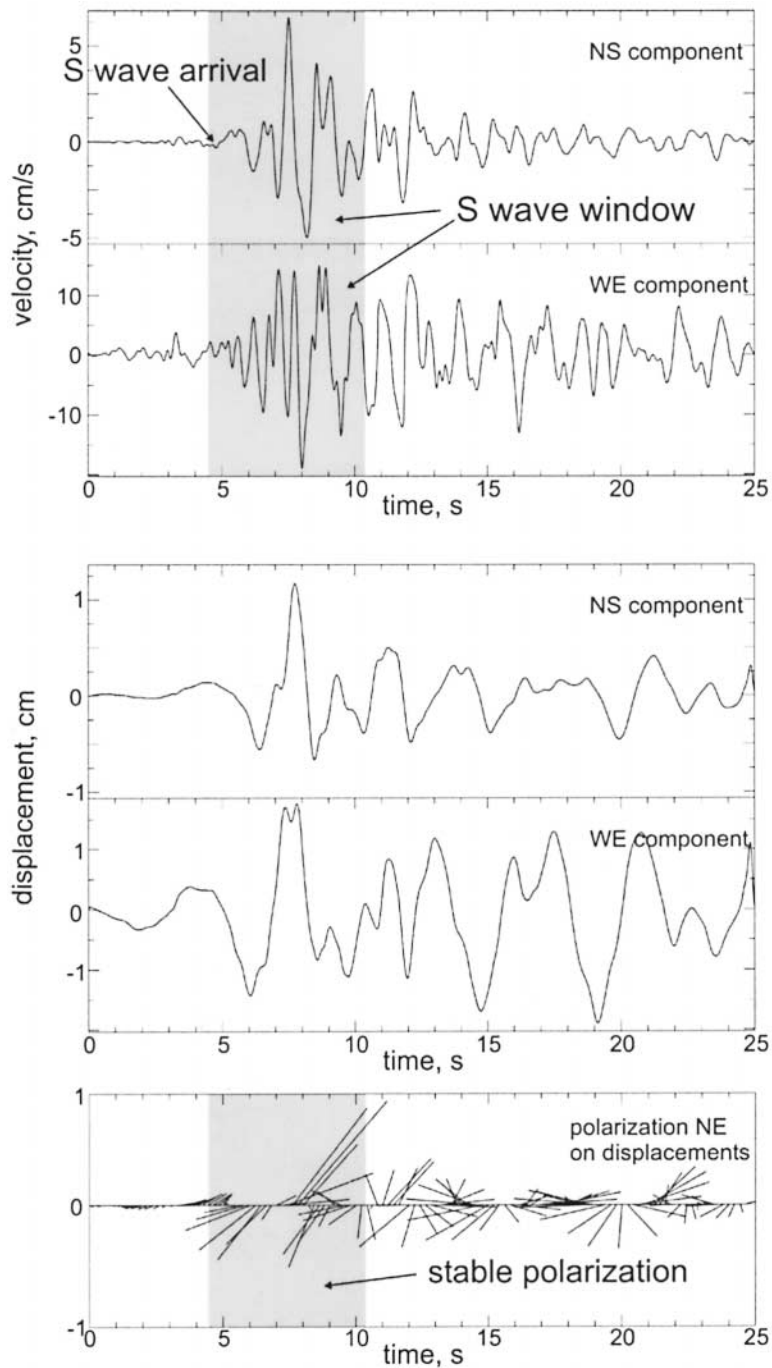


Figure 2. Example of the procedure for the individuation of the direct *S*-wave window in the Hollister station. (Top) Horizontal components of ground velocity in the frequency band 0.5–5 Hz from integration of accelerometric records. (Middle) Horizontal components of ground displacement. (Bottom) *S*-wave polarization evaluated from displacements.

ever, synthetic amplitudes are within a factor 1.5 of the observed ones. The north–south synthetics (Fig. 5) reproduce well the observed complex shape and duration of ground motion at different azimuths and distances (see, for instance, stations SAR, CAP, and GIL4). The overall fit of the west–east components of ground motion (Fig. 6) is worse than for the north–south components, mainly because of the mismatch of stations SJT and COR, whereas for the other stations synthetics match the spatial variation of the low-frequency shape and duration of observed records fairly well. In particular, the remarkable fit of the west–east com-

ponent of station GIL4 must be pointed out. We believe the discrepancies in the waveforms are mainly due to the use of theoretical, inaccurate Green’s functions that do not include either secondary phases or local site effects, which are present, for example, in the CAP, COR, and GIL4 receivers (Chin and Aki, 1991).

#### Error Analysis

Error estimates on the obtained final slip and rupture velocity distributions are addressed in Figure 7A and B. To

Table 3  
Results of the Inversion at the End of the Several Runs Performed

Control Points	Individuals in the Population	No. of Generations	$E$ ( $10^{-2}$ $\text{m}^2 \text{sec}^{-2}$ )	$F$	AICc	$\langle \Delta u \rangle$ (m)	$\langle v_p \rangle$ (m/sec)
$5 \times 3$	400	110	1.095	0.781	3389	0.87	2720
$7 \times 4$	500	140	0.975	0.805	2902	0.87	2790
$8 \times 6$	800	160	0.937	0.813	2801	1.12	2800
$11 \times 6$	900	110	0.900	0.820	2690	1.22	2790
<b><math>15 \times 8</math></b>	<b>1300</b>	<b>250</b>	<b>0.828</b>	<b>0.834</b>	<b>2543</b>	<b>1.44</b>	<b>2790</b>
$17 \times 8$	1400	245	0.820	0.836	2569	1.43	2790

Reported for each run are the number of control points, the number of individuals in the population on which the Genetic Algorithms acted, the number of generations through which the population evolved, the final misfit value (equation 5), the final fitness value (equation 4 with  $E_{\text{MAX}} = 0.05 \text{ m}^2 \text{sec}^{-2}$ ), the AICc value (equation 6), and the mean values on the fault for the final slip and rupture velocity. The values in boldface indicate the best-fit run according to the minimum AICc criterion.

get them we performed the following procedure. Let us consider a particular control point and focus on one of the two parameters, final slip or rupture velocity, defined on it. We perturb the value of this parameter around the final value  $p_{\text{best}}$  we have determined through the inversion, assigning it some values distributed in the range  $[0.9 p_{\text{best}}, 1.1 p_{\text{best}}]$ , that is, in a neighborhood of  $p_{\text{best}}$  wide  $\pm 10\%$  of  $p_{\text{best}}$ . Fixing the whole set of other parameters at their final best value, for each  $p \in [0.9 p_{\text{best}}, 1.1 p_{\text{best}}]$  we compute the misfit  $E(p)$  by equation (5) and then the value for the function

$$pdf(p) = C \exp\left[-\frac{E^2(p)}{2\sigma_0^2}\right], \quad (7)$$

assuming that the expected errors are Gaussian distributed with zero mean. The constant  $C$  in equation (7) is determined requiring that the area under the function is 1:

$$C = \frac{1}{\int_{0.9p_{\text{best}}}^{1.1p_{\text{best}}} \exp\left[-\frac{E^2(p)}{2\sigma_0^2}\right] dp}. \quad (8)$$

In this way the function  $pdf(p)$  assumes the meaning of a marginal probability distribution function for the parameter  $p_{\text{best}}$ . In other words, the estimates of uncertainties on model parameters are obtained from the analysis of the marginal probability distribution functions, that is, the probability for a single parameter  $p_i$  with  $p_j = p_{j,\text{best}}$  and  $i \neq j$  (Jackson and Matsu'ura, 1985; Zollo *et al.*, 2002). This technique is similar to the estimate of the covariance matrix in linear or linearized approaches but considering only its diagonal elements, that is, the parameter variances (Menke, 1989). The parameter  $\sigma_0^2$  in equations (7) and (8) is the unknown variance of the misfit function (5) and accounts for errors both in the modeling and in the data. It determines the shape of

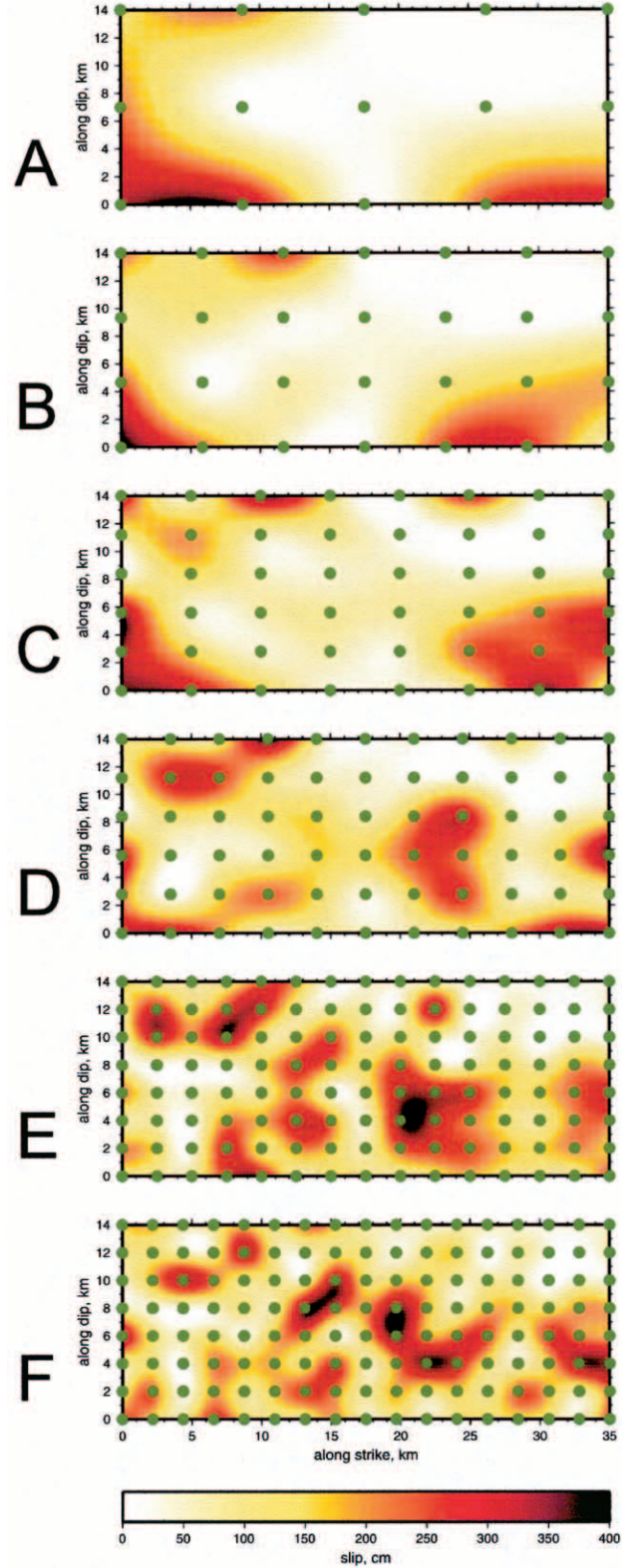


Figure 3. Multiscale search for the final slip distribution on the fault plane. The green dots represent the control points. (A)  $5 \times 3$  grid. (B)  $7 \times 4$  grid. (C)  $8 \times 6$  grid. (D)  $11 \times 6$  grid. (E)  $15 \times 8$  grid. (F)  $17 \times 8$  grid.

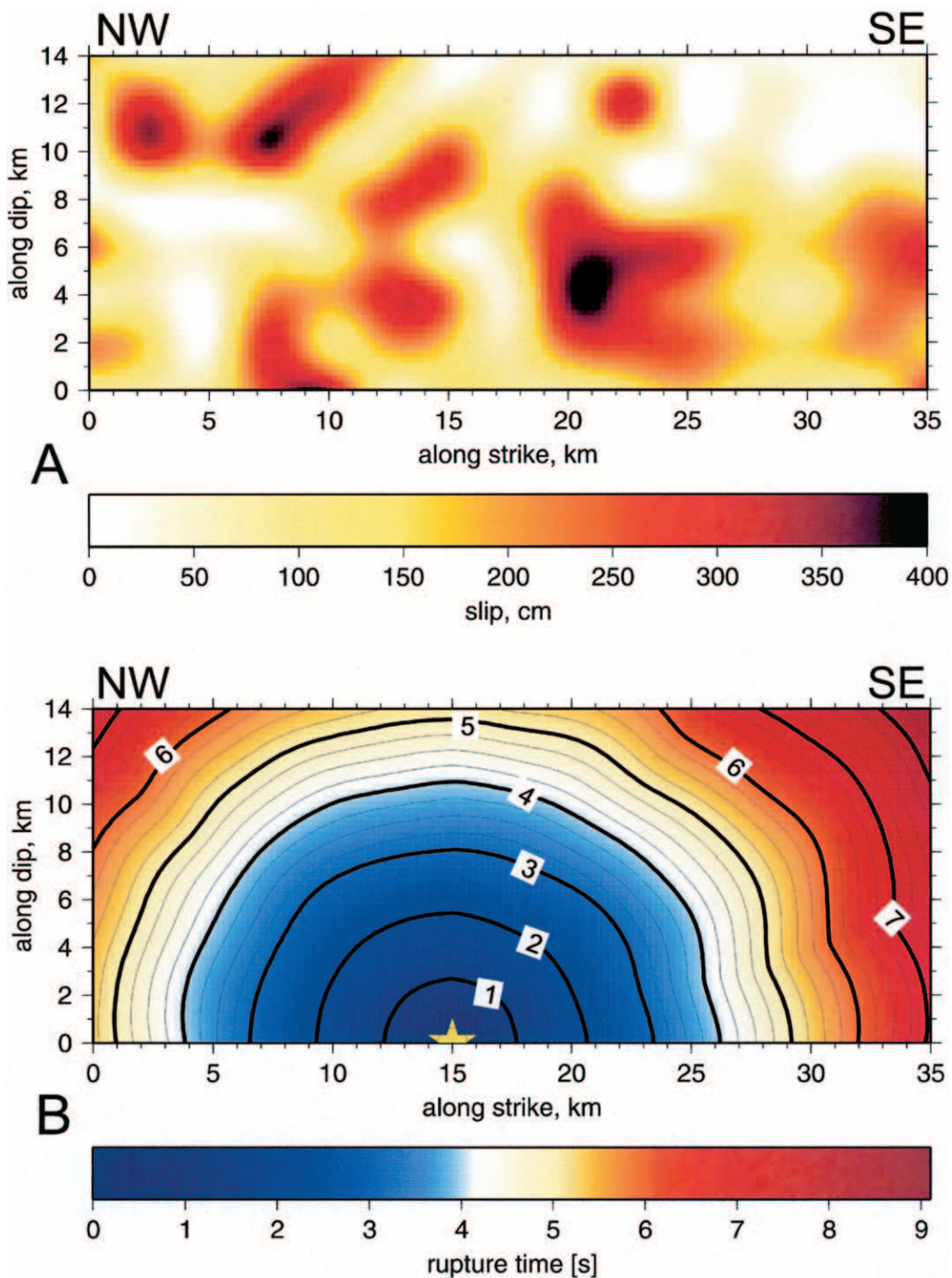


Figure 4. Final slip- (A) and rupture-time (B) distributions on the fault plane for the 1989 Loma Prieta earthquake. In B, the contour intervals are plotted every 0.25 sec, and the star represents the position of the rupture nucleation point.

the *pdf* (7) and, in the present case, it has to be assigned arbitrarily, according to the best-fit model variance (Table 3).

We computed, through the empirical way described previously, the function *pdf* for each control point both for final slip and for rupture velocity. We can characterize these probability distribution functions by their overall widths. One way of measuring the width of a distribution is to multiply

it by a function that is zero near the center of distribution and that grows on either side of center (Menke, 1989). As shown in Figure 8 for a few control points, if the distribution is narrow, then the resulting function will be small everywhere; if the distribution is wide, then the resulting function will be large. A quantitative measure of the width of the distribution is given by the area under the resulting function.

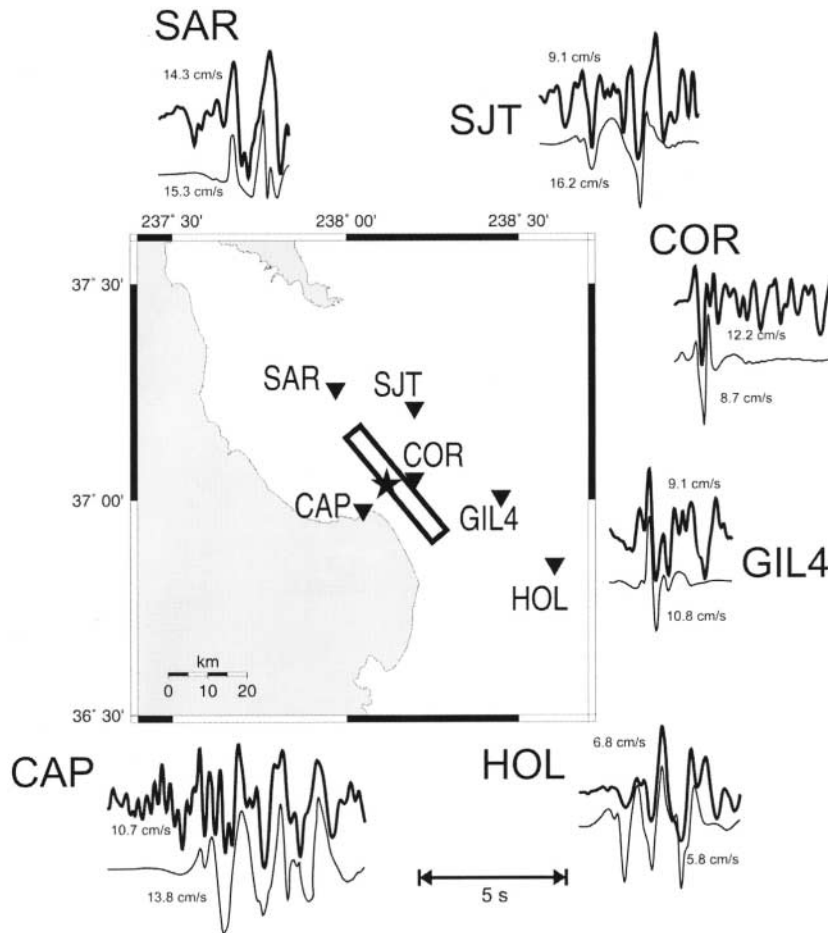


Figure 5. Real (thick lines) and synthetic (thin lines) computed for the best-fit model ground-velocity records for the north-south component in the 0.5 to 5-Hz frequency range. The peak velocity value for each seismogram is also reported.

If one chooses the parabola  $f = (p - p_{\text{best}})^2$  as the function, then this area gives the variance  $\sigma^2$  of the distribution

$$\sigma^2 = \int_{0.9p_{\text{best}}}^{1.1p_{\text{best}}} (p - p_{\text{best}})^2 \text{pdf}(p) dp \quad (9)$$

and then its square root  $\sigma$  is a measure of the width of the distribution and, in other words, a measure of the error associated with  $p_{\text{best}}$ .

In Figure 7A and B we represented the distributions on the fault plane for the relative error  $\sigma(p_{\text{best}})/p_{\text{best}}$ , expressed in percentage, associated, respectively, with the final slip and the rupture velocity. The percentage relative errors on final slip are between 22% and 36%. As we can see in Figure 7A, the smallest relative errors for final slip distribution are found in the central part of the fault, where we retrieved the main asperities (Fig. 7A). In this area the percentage error does not exceed the 25%. We found larger errors for the rupture-velocity distribution. In this case (Fig. 7b) the percentage relative errors are between 21% and 46%. However, errors which do not exceed the 27% are found in the area between the rupture nucleation point and the southeastern edge of the fault. As we said before, in this direction we

retrieved a faster velocity for the rupture front. In the north-western edge of the fault the final slip asperity we found there (Fig. 7A) is characterized by a large error (about 35%). On the contrary, in the same region, the error associated with the rupture velocity is relatively smaller (about 25%). Probably in this zone we are not able to resolve the trade-off between the final slip and the rupture velocity.

#### Comparison with Other Studies

Several authors have proposed an extended faulting model for the Loma Prieta earthquake (Steidl *et al.*, 1991; Zeng *et al.*, 1993; Beroza, 1996; Hartzell *et al.*, 1996; Wald *et al.*, 1996). Although many of the strong motion data analyzed in this article are common to these studies, several differences (e.g., different frequency bands, model parameterizations, inversion methods, approach to the forward problem) can lead to varying results.

First, we briefly review the assumptions used in each of these studies in comparison with ours. Steidl *et al.* (1991) modeled strong motion velocity records from 20 near-source receivers in the frequency range 0.05–1 Hz. The inversion was performed with inequality and smoothness constraints and the forward problem was solved by a complete seismograms approach.

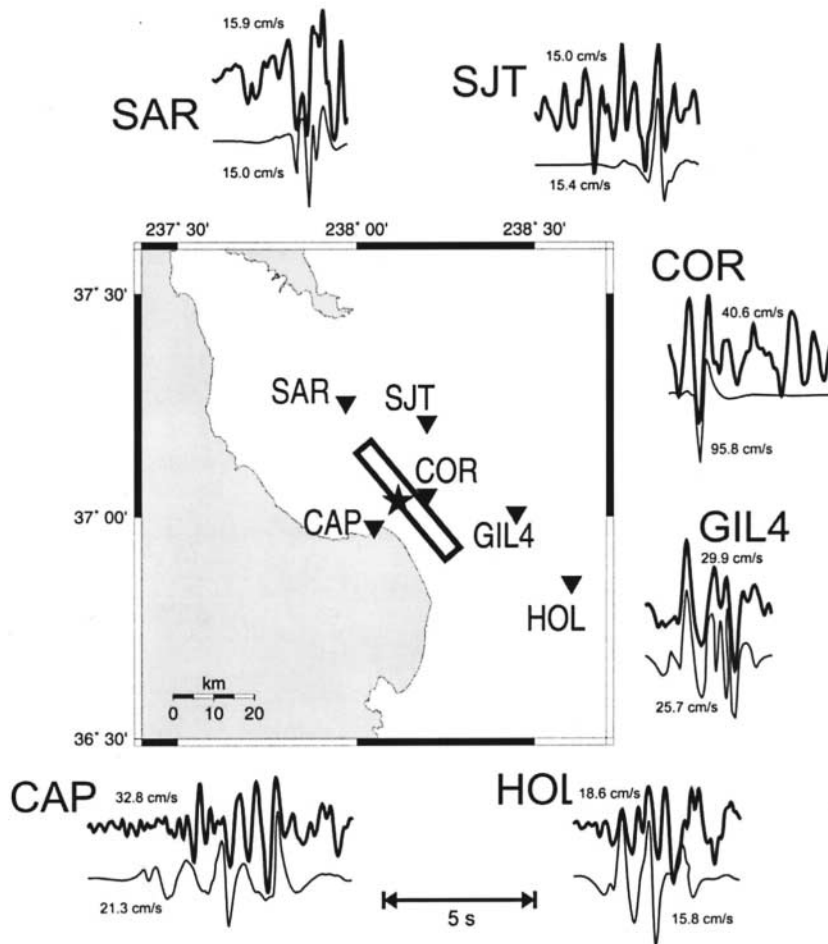


Figure 6. As in Figure 5 except for the west–east components of the ground velocity.

Zeng *et al.* (1993) performed a waveform inversion of horizontal components of displacement strong motion data from 14 stations with an epicentral distance less than 35 km. Using a recursive stochastic inversion method, they determined both the low-frequency final slip distribution from the low-pass filtered data ( $f < 2$  Hz) and the high-frequency energy radiation map from the envelope of the squared high-pass filtered data ( $f > 5$  Hz).

Beroza (1996) used the horizontal components of the displacement in the frequency range 0.33–2 Hz for 20 of the closest strong motion stations. The inversion was performed using a tomographic backprojection approach and the forward problem was solved by using the ray theory in a time-dependent Kirchoff formulation (Spudich and Frazer, 1984).

Hartzell *et al.* (1996) used teleseismic  $P$  waves from 24 stations and  $SH$  body waves from 16 stations in the Global Seismic Network at frequencies above 1 Hz and great-circle distances between  $30^\circ$  and  $90^\circ$ . The inversion was performed using both  $L_1$  and  $L_2$  norms with inequality and smoothness constraints and the forward problem was solved by the generalized ray theory.

Wald *et al.* (1996) used teleseismic  $P$ -wave velocity waveforms from 16 stations, teleseismic  $SH$  velocity wave-

forms from eight stations, and velocity records from 16 near-source stations in the frequency band 0.1–1 Hz. The inversion was performed by using a least-squares method with inequality and smoothness constraints, and seismograms for the forward problem were computed by generalized ray theory and discrete wavenumber/finite-elements technique.

Although there is a certain overlap in the data sets used, the methods differ substantially with respect to the one we propose. Moreover, the frequency bands used include lower frequencies than that we considered. On the other hand our frequency band extends at higher frequencies than those considered in the cited studies. Also we performed a purely nonlinear inversion whereas the inverse problem is linearized in cited methods. In any case, there are several similarities in the map for the total slip amplitude we derived with those obtained by other authors. All the studies find a relatively low slip amplitude in the hypocentral region and a substantially bimodal distribution with respect to the hypocenter. The retrieved seismic moments range from  $2.3 \times 10^{19}$  N m to  $3.5 \times 10^{19}$  N m against the value of  $2.1 \times 10^{19}$  N m we found. These results are all consistent with the range determined by teleseismic data analysis at longer periods.

Differences among the final slip distributions, including

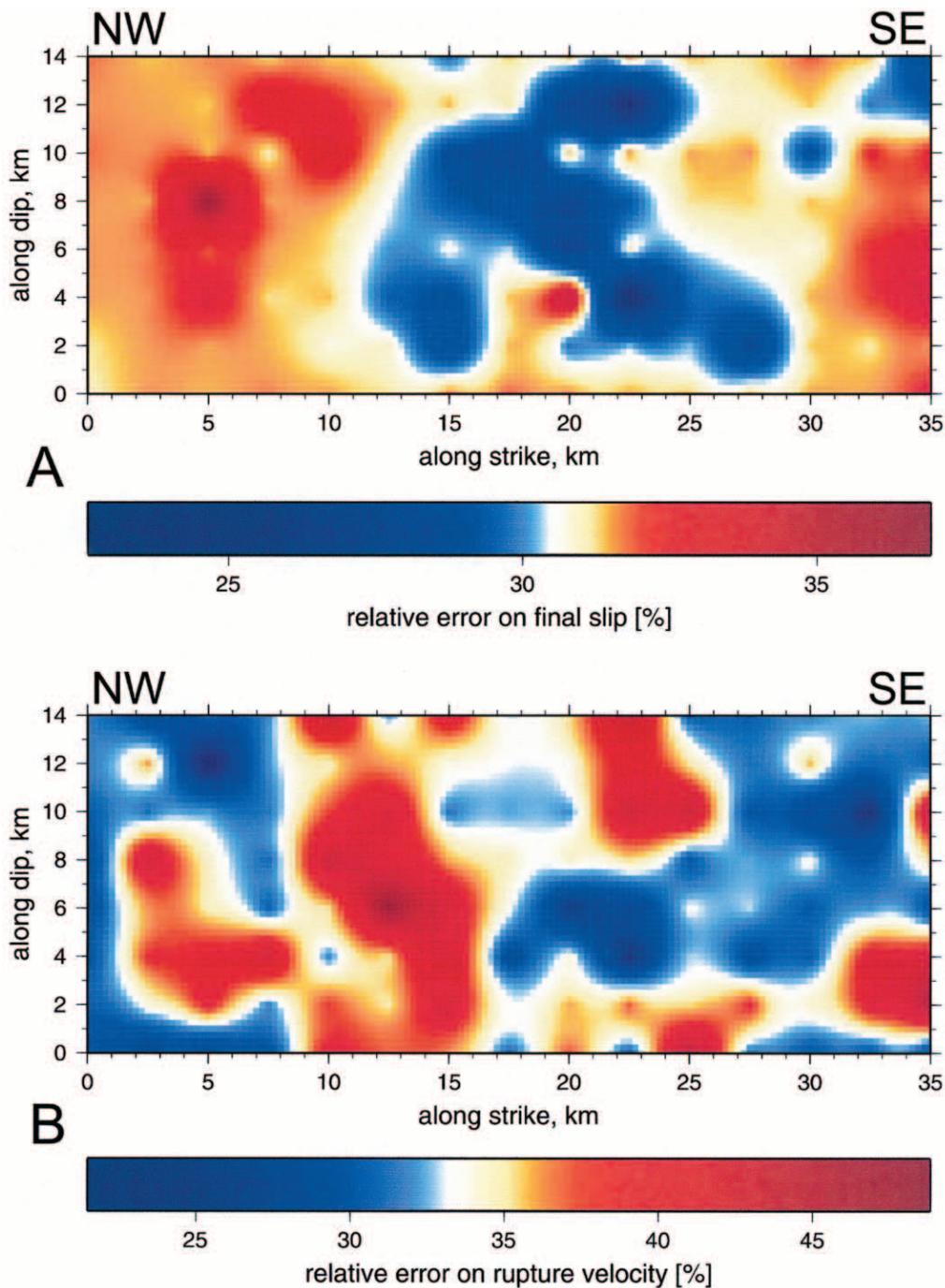


Figure 7. (A) Relative error distribution for the final slip of Figure 2 according to the color scale reported. (B) Relative error distribution for the rupture propagation velocity on the fault according to the color scale reported.

ours, proposed for the Loma Prieta earthquake arise from the data sets used (which can also include teleseismic data) and from the frequency contents considered. A bimodal trend for the final slip on the fault plane is evident for all the proposed models. Our results look fairly similar to those proposed by Zeng *et al.* (1993) and Beroza (1996) who inverted only near-fault strong motion seismograms up to 2 Hz. Steidl *et al.* (1991) also inverted only near-fault strong

motion data, but they performed their inversion at a maximum frequency of 1 Hz, and this leads to differences found especially for the slip peak values associated with the major asperities that can be related to the higher-frequency contributions. Although most results agree on the slip distribution for the Loma Prieta earthquake, they differ significantly regarding the time evolution of the faulting process. Steidl *et al.* (1991) found an average rupture velocity of 3.0 km/sec

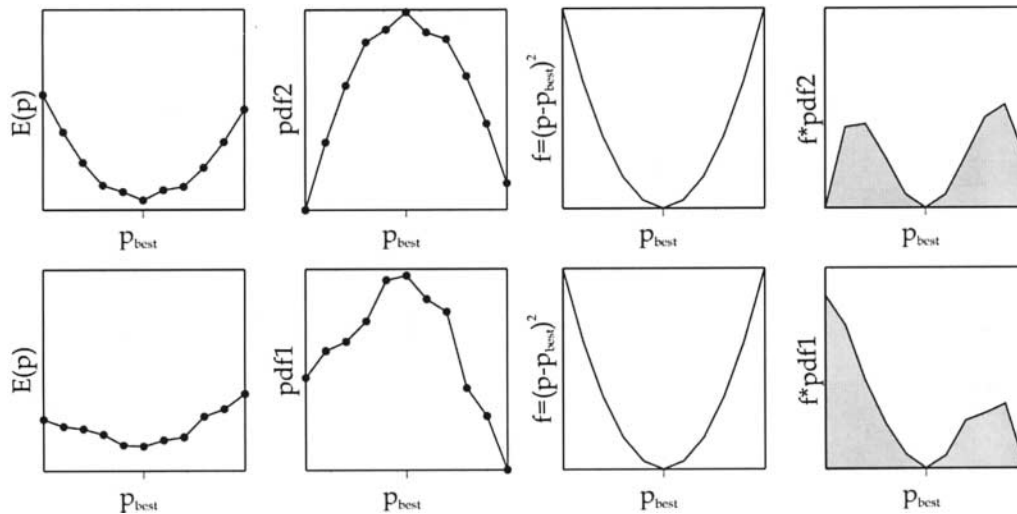


Figure 8. A parabola of the form  $f = (p - p_{\text{best}})^2$  is used to measure of the width of two probability-distribution functions that have the same mean but different widths: the product  $f * \text{pdf}$  is small everywhere for the narrow distribution but has two large peaks for the wider distribution. The area under  $f * \text{pdf}$  is related to the width of the distribution.

with a velocity of 3.4 km/sec for the rupture propagation to the southeast. Zeng *et al.* (1993) tried different rupture-velocity models finding that a rupture velocity of 2.5 km/sec provided the best fit in terms of the Euclidean norm. Beroza (1996) obtained rupture velocities ranging between 2.7 km/sec and 3.1 km/sec, and Wald *et al.* (1996) found a rupture velocity of 2.5 km/sec. Our results show an average rupture velocity of about 2.8 km/sec with a peak velocity of about 3.0 km/sec for the propagation of the rupture to the southeast. All these models, including our model, assume the rupture propagated simultaneously northwest and southeast. On the contrary, Horton *et al.* (1996), using a frequency domain inversion technique that allows much greater freedom in the rupture behavior, found that the rupture to the northwest initiated after the rupture to the southeast and obtained higher rupture velocities ranging between 3.5 and 5 km/sec.

Zeng *et al.* (1993) used their inversion method to map the high-frequency ( $f > 5$  Hz) energy radiation intensity over the fault plane. Their results show that the energy radiation intensity was highly variable and the energy-sources distribution was very different from the final slip map. The most important sources are located near the boundary areas of the large slip zones. In particular, one of these energy patches is located close to the rupture nucleation point where we find a relatively small slip amplitude. They conclude that the earthquake probably started as a small rupture event. The fracture then accelerated and increased in slip amplitude around the source area, producing high-frequency radiation.

### Conclusion

In this article we developed a nonlinear inversion technique of high-frequency data for the simultaneous determi-

nation of slip- and rupture-time distributions on an extended fault.

The kinematic source parameters are determined searching for the minimum of a  $L_2$  norm-based misfit function by the GA (Goldberg, 1989; Charbonneau, 1995). We point out that the use of a truly nonlinear inversion technique, that is, the GA, allows for an exhaustive exploration of the model parameters space. The forward problem, that is, the computation of synthetic seismograms, is solved using the asymptotic ray theory for given final slip- and rupture-time distributions on an extended fault. The rupture velocity and the final slip are determined through data inversion at a set of control points of a bicubic interpolating function on the fault plane, and the distributions over the whole fault are then obtained by interpolation. Rupture times are computed, starting from a given rupture-velocity distribution, through the algorithm of Podvin and Lecomte (1991).

An adaptive model space investigation, according to which the number of control points is progressively increased (multiscale approach), is used to move from the high- to the low-wavelength description of final slip and rupture velocity on the fault plane. The optimal model parameterization is chosen according to the minimum of the corrected Akaike Information Criterion parameter (Akaike, 1974; Cavanaugh, 1997). We applied our inversion technique to invert the horizontal components of six near-fault strong motion records to determine the kinematic source parameters for the 1989 Loma Prieta earthquake. We found two areas of very high slip: one at approximately 7 km southeast of the hypocenter at 12 km depth and another about 8 km northwest of the hypocenter at 10 km depth with peak amplitude of about 4 m and more than 3 m, respectively. As shown by Beroza (1996), these high-slip regions are rela-

tively poor in aftershocks, whereas the low-slip areas are characterized by an aftershocks abundance. The scalar seismic moment we found is approximately equal to  $2.1 \times 10^{19}$  N m, result which agrees both with inversion analysis and with long-period determinations.

Moreover, we found that rupture propagated with an average velocity of about 2.8 km/sec with a higher velocity of about 3.0 km/sec for the propagation to the southeast from the hypocenter. The total duration of the rupture has been estimated equal to about 9 sec, which agrees with the estimation by Beroza (1996).

On the basis of the error analysis performed, we point out that the high-slip regions on the fault plane are characterized by the smallest error and, therefore, they are well constrained. The same conclusion is valid for the high rupture velocity found in the area southeast of the hypocenter, which is characterized by a small error, too. On the other hand, we are not able to resolve the trade-off between rupture velocity and the final slip in the area near the top western edge of the fault, where we found a large final slip characterized by a large error and a low rupture velocity with small errors. Although further investigations of the high-frequency source characteristics of the extended earthquake fault require accounting for effects like site responses, multipathing, and scattering, we believe that our result provides a reliable overall description of the Loma Prieta earthquake source process.

### Acknowledgments

We thank S. Das, L. D'Auria, A. Herrero, R. Madariaga, S. Nielsen, and P. Spudich for their comments, suggestions, and helpful discussions that greatly improved this article. We also thank two anonymous reviewers and the Associate Editor C. Trifu for their thoughtful reviews. We thank G. Festa; this article has profited greatly from ideas we gathered from numerous discussions with him. The figures in this article were made with Generic Mapping Tools (Wessel and Smith, 1991).

### References

- Akaike, H. (1974). A new look at the statistical model identification, *IEEE Trans. Autom. Control* **6**, 716–723.
- Aki, K., and P. G. Richards (1980). *Quantitative Seismology, Theory and Methods* (2 volumes). W. H. Freeman, San Francisco, 932 pp.
- Anderson, J. G. (1991). Strong motion seismology, *Rev. Geophys.* (suppl.), **29**, 700–720.
- Archuleta, R. J. (1984). A faulting model for the 1970 Imperial Valley earthquake, *J. Geophys. Res.* **89**, 4559–4585.
- Azimi, Sh. A., A. V. Kalinin, V. V. Kalinin, and B. L. Pivovarov (1968). Impulse and transient characteristics of media with linear and quadratic absorption laws, *Izv. Phys. Solid Earth* **2**, 88–93.
- Barker, J. S., and D. H. Salzberg (1990). Long-period and broad-band teleseismic body waves modelling of the October 17, 1989 Loma Prieta earthquake, *Geophys. Res. Lett.* **17**, 1409–1412.
- Bernard, P., and R. Madariaga (1984). A new asymptotic method for the modelling of near-field accelerograms, *Bull. Seism. Soc. Am.* **74**, 539–557.
- Beroza, G. C. (1996). Rupture history of the earthquake from high frequency strong motion data, in *The Loma Prieta, California, earthquake of October 17, 1989—main shock characteristics*, U.S. Geol. Surv. Profess. Pap. 1550-A, P. Spudich (Editor), 9–32.
- Beroza, G. C., and P. Spudich (1988). Linearized inversion for fault rupture behaviour: application to the 1984 Morgan Hill, California, earthquake, *J. Geophys. Res.* **93**, 6275–6296.
- Boatwright, J., J. B. Fletcher, and T. E. Fumal (1991). A general inversion scheme for source, site, and propagation characteristics using multiply recorded sets of moderate-sized earthquakes, *Bull. Seism. Soc. Am.* **81**, 1754–1782.
- Boschetti, F., M. C. Dentith, and R. D. List (1996). Inversion of seismic refraction data using genetic algorithms, *Geophysics* **61**, 1715–1727.
- Bouchon, M. (1979). Discrete wavenumber representation of elastic wave field in three space dimension, *J. Geophys. Res.* **84**, 3609–3614.
- Bouchon, M. (2003). A review of the discrete wavenumber method, *Pure Appl. Geophys.* **160**, 445–465.
- Bouchon, M., M. N. Toksöz, H. Karabulut, M. P. Bouin, M. Dietrich, M. Aktar, and M. Edie (2002). Space and time evolution of rupture and faulting during the 1999 Izmit (Turkey) earthquake, *Bull. Seism. Soc. Am.* **92**, 256–266.
- Bunks, C., F. M. Saleck, S. Zaleski, and G. Chavent (1995). Multi-scale seismic waveform inversion, *Geophysics* **60**, 1457–1473.
- Cavanaugh, J. E. (1997). Unifying the derivation for the Akaike and corrected Akaike Information Criteria, *Stat. Probabil. Lett.* **33**, 201–208.
- Charbonneau, P. (1995). Genetic algorithms in astronomy and astrophysics, *Astrophys. J.* **101** (suppl.), 309–334.
- Chin, B. H., and K. Aki (1991). Simultaneous study of source, path, and site effects on strong ground motion during the 1989 Loma Prieta earthquake: a preliminary results on pervasive non linear site effects, *Bull. Seism. Soc. Am.* **81**, 1859–1884.
- Choy, G. L., and J. Boatwright (1990). Source characteristics of the Loma Prieta, California earthquake of October 18, 1989 from global digital seismic data, *Geophys. Res. Lett.* **17**, 1183–1186.
- Dietz, L. D., and W. L. Ellsworth (1990). The October 17, 1989 Loma Prieta, California, earthquake and its aftershocks; geometry of the sequence from high resolution location, *Geophys. Res. Lett.* **17**, 1417–1420.
- Emolo, A. (2001). Modelli di frattura dei terremoti crostali di media e forte magnitudo dall'inversione non lineare di registrazioni a corto-periodo, *Ph.D. Thesis in Geophysics*, Università "Federico II" di Napoli, Italy (in Italian).
- Farra, V., and R. Madariaga (1987). Seismic waveform modelling in heterogeneous media by ray perturbation theory, *J. Geophys. Res.* **92**, 2697–2712.
- Farra, V., P. Bernard, and R. Madariaga (1986). Fast near source evaluation of strong motion for complex source models, in *Earthquake Source Mechanics*, American Geophysical Monograph 37, S. Das, J. Boatwright, and C. H. Scholz (Editors), 121–130.
- Goldberg, D. E. (1989). *Genetic Algorithms in Search, Optimization and Machine Learning*, Addison-Wesley, New York, 432 pp.
- Hartzell, S. H. (1978). Earthquake aftershocks as Green's function, *Geophys. Res. Lett.* **5**, 1–4.
- Hartzell, S. H., G. S. Stewart, and C. Mendoza (1996). Comparison of  $L_1$  and  $L_2$  norms in teleseismic waveform inversion for the rupture history of the earthquake, in *The Loma Prieta, California, earthquake of October 17, 1989—main shock characteristics*, U.S. Geol. Surv. Profess. Pap. 1550-A, P. Spudich (Editor), 39–57.
- Heaton, T. H. (1990). Evidence for and implications of self-healing pulses of slip in earthquake rupture, *Phys. Earth Planet. Interiors* **64**, 1–20.
- Horton, S. P., J. G. Anderson, and A. J. Mendez (1996). Frequency domain inversion for the rupture characteristics during the earthquake, using strong motion data and geodetic observations, in *The Loma Prieta, California, earthquake of October 17, 1989—main shock characteristics*, U.S. Geol. Surv. Profess. Pap. 1550-A, P. Spudich (Editor), 59–73.
- Hutchings, L. (1994). Kinematic earthquake models and synthesized ground motion using empirical Green's functions, *Bull. Seism. Soc. Am.* **84**, 1028–1050.
- Irikura, K. (1986). Prediction of strong acceleration motion using empirical

- Green's function, in *Proc. of 7th Japan Earthquake Engineering Symposium*, Tokyo, Japan, 10–12 December 1986, 151–156.
- Jackson, D. D., and M. Matsu'ura (1985). A bayesian approach to non linear inversion, *J. Geophys. Res.* **90**, 581–591.
- Jin, S., and W. Beydoun (2000). 2D multi-scale non-linear velocity inversion, *Geophys. Prospect.* **48**, 163–180.
- Kanamori, H., and K. Satake (1990). Broadband study of the 1989 Loma Prieta earthquake, *Geophys. Res. Lett.* **17**, 1179–1182.
- Koyama, J. (1997). *The Complex Faulting Process of Earthquakes*, Kluwer Academic, Dordrecht, The Netherlands, 194 pp.
- Langston, C. A., K. P. Furlong, K. S. Vogfjord, R. H. Clouser, and C. J. Ammon (1990). Analysis of teleseismic body waves radiated from the Loma Prieta earthquake, *Geophys. Res. Lett.* **17**, 1405–1408.
- Lutter, W. J., R. L. Nowack, and L. W. Braille (1990). Seismic imaging of upper crustal structure using travel times from the PASSCAL Ouchita experiment, *J. Geophys. Res.* **95**, 4621–4631.
- Menke, W. (1989). *Geophysical Data Analysis: Discrete Inverse Theory*, Academic Press, San Diego, 285 pp.
- Podvin, P., and I. Lecomte (1991). Finite difference computation of travel times in very contrasted velocity models: a massively parallel approach and its associated tools, *Geophys. J. Int.* **105**, 793–804.
- Romanowicz, B. A., and H. Lyon-Caen (1990). The Loma Prieta earthquake of October 18, 1989; results of teleseismic mantle and body waves inversion, *Geophys. Res. Lett.* **17**, 1191–1194.
- Ruff, L. J., and B. W. Tichelaar (1990). Moment tensor rate functions for the 1989 Loma Prieta earthquake, *Geophys. Res. Lett.* **17**, 1187–1190.
- Sambridge, M., and G. Drijkoningen (1992). Genetic algorithms in seismic waveform inversion, *Geophys. J. Int.* **109**, 323–342.
- Somerville, P., and J. Yoshimura (1990). The influence of critical Moho reflections on strong ground motions recorded in San Francisco and Oakland during the 1989 Loma Prieta earthquake, *Geophys. Res. Lett.* **17**, 1203–1206.
- Spudich, P., and L. N. Frazer (1984). Use of ray theory to calculate high-frequency radiation from earthquake source having spatially variable rupture velocity and stress drop, *Bull. Seism. Soc. Am.* **74**, 2061–2082.
- Steidl, J. H., R. J. Archuleta, and S. H. Hartzell (1991). Rupture history of the 1989 Loma Prieta, California, earthquake, *Bull. Seism. Soc. Am.* **81**, 1573–1602.
- U.S. Geological Survey (1990). The Loma Prieta, California, earthquake; an anticipated event. *Science* **247**, 286–293.
- Wald, D. J., T. H. Heaton, and D. V. Helmberger (1996). Strong-motion and broadband teleseismic analysis of the earthquake for rupture process and hazard assessment, in *The Loma Prieta, California, earthquake of October 17, 1989—main shock characteristics*, U.S. Geol. Surv. Profess. Pap. 1550-A, P. Spudich (Editor), 235–262.
- Wessel, P., and W. H. F. Smith (1991). Free software helps map and display data, *EOS Trans. AGU* **72**, 441, 445–446.
- Zeng, Y., K. Aki, and T. Teng (1993). Mapping of the high-frequency source radiation for the Loma Prieta earthquake, California, *J. Geophys. Res.* **98**, 11,981–11,993.
- Zhang, J., and T. Lay (1990). Source parameters of the 1989 Loma Prieta earthquake determined from long-period Rayleigh waves, *Geophys. Res. Lett.* **17**, 1195–1198.
- Zhang, W., T. Iwata, K. Irikura, H. Sekiguchi, and M. Bouchon (2003). Heterogeneous distribution of the dynamic source parameters of the 1999 Chi-Chi, Taiwan, earthquake, *J. Geophys. Res.* **108**, 2232, doi 10.1029/2002JB001889.
- Zollo, A., A. Bobbio, A. Emolo, A. Herrero, and G. De Natale (1997). Modelling of the ground acceleration filed in the near source range: the case of the 1976 Friuli earthquake ( $M = 6.5$ ), Northern Italy, *J. Seism.* **1**, 305–319.
- Zollo, A., L. D'Auria, R. De Matteis, A. Herrero, J. Virieux, and P. Gasparini (2002). Bayesian estimation of 2-D P-velocity models from active seismic arrival time data: imaging of the shallow structure of Mt. Vesuvius (Southern Italy), *Geophys. J. Int.* **151**, 566–582.

Dipartimento di Scienze Fisiche  
 Università "Federico II" di Napoli  
 Napoli, Italy 80126

Manuscript received 15 September 2003.